All-digital wavefront sensing for structured light beams

Angela Dudley,[1,*] **Giovanni Milione,**[2,3,4] **Robert R. Alfano,**[2,3,4] **and Andrew Forbes**[1,5]

[1]*CSIR National Laser Centre, PO Box 395, Pretoria 0001, South Africa*
[2]*Institute for Ultrafast Spectroscopy and Lasers, Physics Department, CUNY City College, 160 Convent Ave., New York, NY 10031 USA*
[3]*Physics Department, CUNY Graduate Center, 365 Fifth Ave., New York, NY 10016 USA*
[4]*New York State Center for Complex Light, 160 Convent Ave., New York, NY 10031 USA*
[5]*School of Chemistry and Physics, University of KwaZulu-Natal, Private Bag X54001, Durban 4000, South Africa*

[*]*adudley@csir.co.za*

Abstract: We present a new all-digital technique to extract the wavefront of a structured light beam. Our method employs non-homogeneous polarization optics together with dynamic, digital holograms written to a spatial light modulator to measure the phase relationship between orthogonal polarization states in real-time, thereby accessing the wavefront information. Importantly, we show how this can be applied to measuring the wavefront of propagating light fields, over extended distances, without any moving components. We illustrate the versatility of the tool by measuring propagating optical vortices, Bessel, Airy and speckle fields. The comparison of the extracted and programmed wavefronts yields excellent agreement.

OCIS codes: (140.3295) Laser beam characterization; (010.7350) Wave-front sensing; (120.5050) Phase measurement; (090.1995) Digital holography; (050.4865) Optical vortices.

References and links

1. B. Hermann, E. J. Fernndez, A. Unterhuber, H. Sattmann, A. F. Fercher, W. Drexler, P. M. Prieto, and P. Artal, "Adaptive optics ultrahigh-resolution optical coherence tomography," Opt. Lett. **29**, 2142–2144 (2004).
2. A. Roorda, F. Romero-Borja, I. William Donnelly, H. Queener, T. Hebert, and M. Campbell, "Adaptive optics scanning laser ophthalmoscopy," Opt. Express **10**, 405–412 (2002).
3. M. A. A. Neil, R. Juakaitis, M. J. Booth, T. Wilson, T. Tanaka, and S. Kawata, "Adaptive aberration correction in a twophoton microscope," J. Microsc. **200**, 105–108 (2000).
4. M. Rueckel, J. A. Mack-Bucher, and W. Denk, "Adaptive wavefront correction in two-photon microscopy using coherence-gated wavefront sensing," Proc. Natl. Acad. Sci. **103**, 17137–17142 (2006).
5. M. Booth, M. Neil, and T. Wilson, "Aberration correction for confocal imaging in refractive-index-mismatched media," J. Microsc. **192**, 90–98 (1998).
6. J. C. Ricklin and F. M. Davidson, "Atmospheric turbulence effects on a partially coherent Gaussian beam: implications for free-space laser communication," J. Opt. Soc. Am. A **19**, 1794–1802 (2002).
7. F. Roddier, M. Séchaud, G. Rousset, P.-Y. Madec, M. Northcott, J.-L. Beuzit, F. Rigaut, J. Beckers, D. Sandler, P. Lena, and O. Lai, *Adaptive Optics in Astronomy* (Cambridge University, 1999).
8. M. Paurisse, M. Hanna, F. Druon, and P. Georges, "Wavefront control of a multicore ytterbium-doped pulse fiber amplifier by digital holography," Opt. Lett. **35**, 1428–1430 (2010).
9. R. Navarro and E. Moreno-Barriuso, "Laser ray-tracing method for optical testing," Opt. Lett. **24**, 951–953 (1999).
10. S. R. Chamot, C. Dainty, and S. Esposito, "Adaptive optics for ophthalmic applications using a pyramid wavefront sensor," Opt. Express **14**, 518–526 (2006).
11. M. P. Rimmer and J. C. Wyant, "Evaluation of large aberrationsusing a lateral-shear interferometer having variable shear," Appl. Opt. **14**, 142–150 (1975).

#211246 - $15.00 USD Received 1 May 2014; revised 23 May 2014; accepted 23 May 2014; published 30 May 2014

12. S. Velghe, J. Primot, N. Guérineau, M. Cohen, and B. Wattellier, "Wave-front reconstruction from multidirectional phase derivatives generated by multilateral shearing interferometers," Opt. Lett. **30**, 245–247 (2005).
13. J. Millerd, N. Brock, J. Hayes, M. North Morris, M. Novak and J. Wyant, "Pixelated phase-mask dynamic interferometer," Proc. SPIE **5531**, 304–314 (2004).
14. M. North Morris, J. Millerd, N. Brock, J. Hayes, B. Saif, "Dynamic Phase-Shifting Electronic Speckle Pattern Interferometer," Proc. SPIE **5869**, 58691B (2005).
15. R. G. Lane and M. Tallon, "Wave-front reconstruction using a Shack-Hartmann sensor," Appl. Opt. **31**, 6902–6908 (1992).
16. C. Schulze, D. Naidoo, D. Flamm, O. A. Schmidt, A. Forbes, and M. Duparré, "Wavefront reconstruction by modal decomposition," Opt. Express **20**, 19714–19725 (2012).
17. C. Schulze, A. Dudley, D. Flamm, M. Duparré, and A. Forbes, "Reconstruction of laser beam wavefronts based on mode analysis," App. Opt. **52**(21), 5312–5317 (2013).
18. G. G. Stokes, "On the composition and resolution of streams of polarized light from different sources," Trans. Cambridge Philos. Soc., **96**, 399 (1852).
19. G. G. Stokes, *Mathematical and Physical Papers* (Cambridge University, 1922).
20. I. Freund, "Poincaré vortices," Opt. Lett. **26**, 1996–1998 (2001).
21. V. Denisenko, A. Minovich, A. Desyatnikov, W. Krolikowski, M. Soskin, and Y. Kivshar, "Mapping phases of singular scalar light fields," Opt. Lett. **33**, 89–91 (2008).
22. I. Freund, A. I. Mokhun, M. S. Soskin, O. V. Angelsky, and I. I. Mokhun, "Stokes singularity relations," Opt. Lett. **27**, 545–547 (2002).
23. S. Vyas, Y. Kozawa, and S. Sato, "Polarization singularities in superposition of vector beams," Opt. Express **21**(7), 8972–8986 (2013).
24. H. Yan and B. Lü, "Spectral Stokes singularities of stochastic electromagnetic beams," Opt. Lett. **34**(13), 1933–1935 (2009).
25. H. Yan and B. Lü, "Propagation of spectral Stokes singularities of stochastic electromagnetic beams through an astigmatic lens," J. Opt. Soc. Am. B **27**(3), 375–381 (2010).
26. Y. Luo and B. Lü, "Spectral Stokes singularities of partially coherent radially polarized beams focused by a high numerical aperture objective," J. Opt. **12**, 115703(2010).
27. O. Korotkova and E. Wolf, "Generalized Stokes parameters of random electromagnetic beams," Opt. Lett. **30**(2), 198–200 (2005).
28. D. Andrews, *Structured Light and Its Applications* (Academic, 2011).
29. A. Forbes, *Laser Beam Propagation: Generation and Propagation of Customized Light* (CRC, 2013).
30. Y. Li, J. Kim, and M. J. Escuti, "Orbital angular momentum generation and mode transformation with high efficiency using forked polarization gratings," Appl. Opt. **51**, 8236–8245 (2012).
31. A. Dudley, Y. Li, T. Mhlanga, M. Escuti, and A. Forbes, "Generating and measuring nondiffracting vector Bessel beams," Opt. Lett. **38**(17), 3429–3432 (2013).
32. D. Goldstein, *Polarized Light* (Marcel Dekker, 2004).
33. C. Schulze, D. Flamm, M. Duparré, and A. Forbes, "Beam-quality measurements using a spatial light modulator," Opt. Lett., **37**(22), 4687–4689 (2012).
34. G. Thalhammer, R. W. Bowman, G. D. Love, M. J. Padgett, and M. Ritsch-Marte, "Speeding up liquid crystal SLMs using overdrive with phase change reduction," Opt. Express **21**(2), 1779–1797 (2013).
35. D. Flamm , C. Schulze, D. Naidoo, S. Schröter, A. Forbes, and M. Duparré, "All-digital holographic tool for mode excitation and analysis in optical fibers," J. Lightwave Technol. **31**(7), 1023–1032 (2013).
36. D. Flamm, O. A. Schmidt, C. Schulze, J. Borchardt, T. Kaiser, S. Schröter, and M. Duparré, "Measuring the spatial polarization distribution of multimode beams emerging from passive step-index large-mode area fibers," Opt. Lett. **35**, 3429–3431 (2010).
37. Q. Cui, M. Li, Z.Yu, "Influence of topological charges on random wandering of optical vortex propagating through turbulent atmosphere," Opt. Comm. **329**, 10–14 (2014).

1. Introduction

Optical aberrations are inevitable in nearly all optical systems, leading to the quest for efficient and precise measurement techniques of the phase or wavefront of an optical field. Accurate wavefront estimation is significant in areas such as ophthalmology [1, 2], microscopy [3–5], free-space communication [6] and astronomy [7]. Laser material processing also relies heavily on wavefront contol as unwanted aberrations can hinder beam quality necessary for cutting and drilling [8]. Some conventional and state-of-the-art methods to extract the wavefront of an optical field exist, ranging from ray tracing [9], pyramid sensors [10], interferometers [11–14], the Shack-Hartmann sensor [15], to the use of correlation filters [16] via modal decomposition

#211246 - $15.00 USD Received 1 May 2014; revised 23 May 2014; accepted 23 May 2014; published 30 May 2014

[17]. However, these techniques are often over-complicated and some of them are unable to detect phase singularities due to an absence of light at the singularity.

To extract the individual phase singularities present in a sample beam, Stokes polarimetry [18, 19] can be performed once the linearly polarized ($y-$axis) sample beam is interfered with a $x-$polarized reference beam [20]. This approach, to exploit the amplitude and phase relationship between orthogonal states of polarization, has been implemented on scalar fields to resolve the topology of neutral pairs of closely positioned phase singularities in speckle fields [21]. Apart from implementing Stokes polarimetry to investigate phase singularities, it can be used to study polarization singularities in coherent beams [22,23] and stochastic electromagnetic beams [24,25] as well as partially coherent radially polarized beams [26] by using the spectral Stokes parameters [27]. Although these techniques can reconstruct closely spaced singularities, they require the manual adjustment of various optical components for the extraction of the Stokes parameters. Moreover, these techniques are designed to measure the wavefront at a fixed plane. Consequently, no study to date has measured wavefronts of propagating fields over extended distances in real-time.

In this work we control the dynamic and geometric phase of light to construct an adjustment-free scheme for the real-time measurement of propagating wavefronts. We devise a novel approach that employs non-homogeneous polarization optics together with digital holograms encoded on a spatial light modulator (SLM). Since these holograms are dynamic, we can demonstrate for the first time Stokes polarimetry in real-time on propagating beams. We illustrate the robustness of our technique by measuring the wavefront of a variety of static and propagating structured light beams [28, 29] such as vortex, Bessel, Airy and speckle fields. We demonstrate that we can reconstruct wavefronts with very high fidelity and resolution which allows us to observe the movement of optical vortices during propagation. Our approach is likely to be useful for the characterization of structured and vector light fields.

2. Theory and concept

While the theory behind Stokes polarimetry is well known, we briefly outline it here for the benefit of the reader. Concurrently, we will illustrate how novel additions to the standard Stokes measurements, namely (1) the inclusion of non-homogeneous polarization optics in the form of a polarization grating (PG) [30, 31] and (2) encoding the SLM to mimic homogeneous polarization optics (such as a quarter-waveplate), can transform this manual-based procedure to an all-digital one. A further departure point is that the SLM can also be used to propagate the field under study, so that the wavefront measurements can be done over extended propagation distances without any moving parts.

First, consider the incoherent superposition between two optical fields of orthogonal polarization states, e.g. horizontal and vertical, representing a vector field

$$\tilde{\mathbf{U}}(r,\phi) = \tilde{\mathbf{U}}_{\leftrightarrow}(r,\phi) + \tilde{\mathbf{U}}_{\updownarrow}(r,\phi), \tag{1}$$

where:

$$\tilde{\mathbf{U}}_{\leftrightarrow}(r,\phi) = |U_{\leftrightarrow}(r,\phi)|\exp(i\delta_{\leftrightarrow}(r,\phi))\hat{\mathbf{x}} \quad \text{and} \quad \tilde{\mathbf{U}}_{\updownarrow}(r,\phi) = |U_{\updownarrow}(r,\phi)|\exp(i\delta_{\updownarrow}(r,\phi))\hat{\mathbf{y}} \tag{2}$$

are the horizontally and vertically polarized components, respectively. $\hat{\mathbf{x}}$ ($\hat{\mathbf{y}}$) are unit vectors parallel (perpendicular) to the propagation axis. $|U_{\leftrightarrow}(r,\phi)|$ and $|U_{\updownarrow}(r,\phi)|$ are amplitudes, and $\delta_{\leftrightarrow}(r,\phi)$ and $\delta_{\updownarrow}(r,\phi)$ are phases of the horizontal and vertical components, respectively. Let's define the phase difference between the horizontal and vertical components as $\delta(r,\phi) = \delta_{\leftrightarrow}(r,\phi) - \delta_{\updownarrow}(r,\phi)$. The vector light field (of Eq. (1)) has a spatially inhomogeneous state of polarization given by the equation:

$$\tilde{\mathbf{U}}(r,\phi) = |U_{\leftrightarrow}(r,\phi)|\hat{\mathbf{x}} + |U_{\updownarrow}(r,\phi)|\hat{\mathbf{y}}\exp(i\delta(r,\phi)), \tag{3}$$

#211246 - $15.00 USD Received 1 May 2014; revised 23 May 2014; accepted 23 May 2014; published 30 May 2014

illustrating that the state of polarization is different at every spatial point (r,ϕ). In general, the state of polarization at a spatial point (r,ϕ) can be described by a polarization ellipse, where the angle of orientation of the polarization ellipse is given by $\delta(r,\phi)$.

We can assign one of the polarization states (vertical) to represent the field of interest, i.e. the field whose wavefront, $\delta(r,\phi)$, we wish to reconstruct, while the other orthogonal polarization state (horizontal) can represent a reference field with a known (or flat) wavefront, for example:

$$\mathbf{U}_{\leftrightarrow}(r,\phi) = \exp\left(-r^2/\omega_0\right) \text{ and } \mathbf{U}_{\updownarrow}(r,\phi) = \exp\left(-r^2/\omega_0\right)\exp\left(i\delta(r,\phi)\right). \tag{4}$$

Here each component consists of a common Gaussian field, while the vertical component has an additional phase term [$\exp(i\delta(r,\phi))$]. Most liquid crystal on silicon (LCOS) SLMs only diffract the vertical component of an incident field into the off-axis, diffraction orders which possess the encoded phase profile. The horizontal component remains impervious to the encoded phase profile in the on-axis, undiffracted order. This can be referred to as "diffraction-inefficiency". We exploit the diffraction-inefficiency to experimentally realise the fields such as those in Eq. (4). A linearly polarized Gaussian beam illuminating the liquid crystal display (LCD) of a SLM encoded with the phase profile, $\exp(i\delta(r,\phi))$, will modify the phase of only the vertical component by $\delta(r,\phi)$, while the horizontal component remains unchanged as depicted in Eq. (4). Consequently, the incoherent mixture of the two components after the SLM can be described in general by Eq. (1) where the weightings of the two modes can be controlled by adjusting the orientation of the polarization state of the field illuminating the LCD via the use of a polarizer.

The extraction of the phase difference between the horizontal and vertical components ($\delta(r,\phi)$) can be achieved via Stokes polarimetry which necessitates four separate intensity profile measurements [32]:

$$\begin{aligned}
S_0(r,\phi) &= |U_{\leftrightarrow}(r,\phi)|^2 + |U_{\updownarrow}(r,\phi)|^2 &&= I_{0^\circ} + I_{90^\circ}\\
S_1(r,\phi) &= |U_{\leftrightarrow}(r,\phi)|^2 - |U_{\updownarrow}(r,\phi)|^2 &&= I_{0^\circ} - I_{90^\circ}\\
S_2(r,\phi) &= 2|U_{\leftrightarrow}(r,\phi)||U_{\updownarrow}(r,\phi)|\cos(\delta(r,\phi)) &&= I_{45^\circ} - I_{135^\circ}\\
S_3(r,\phi) &= 2|U_{\leftrightarrow}(r,\phi)||U_{\updownarrow}(r,\phi)|\sin(\delta(r,\phi)) &&= I_R - I_L
\end{aligned} \tag{5}$$

The Stokes parameters are directly related to the polarization ellipse; in terms of the Stokes parameters, the angle of orientation and the ellipticity of the polarization ellipse at every spatial point (r,ϕ) are given, respectively, by the equations [32]:

$$\alpha(r,\phi) = \arctan\left(\frac{S_2(r,\phi)}{S_1(r,\phi)}\right) \quad \text{and} \quad \delta(r,\phi) = \frac{1}{2}\arctan\left(\frac{S_3(r,\phi)}{S_2(r,\phi)}\right). \tag{6}$$

The salient feature of Eq. (6) is that the phase difference $\delta(r,\phi)$ between the horizontal and vertical components of a vector light field at a point (r,ϕ) is completely described by the ellipticity of the corresponding polarization ellipse at that point. In turn, the ellipticity of the polarization ellipse is completely described by the Stokes parameters $S_3(r,\phi)$ and $S_2(r,\phi)$ which are easily measured via intensity measurements. Therefore, the phase difference $\delta(r,\phi)$ between the horizontal and vertical components is easily measured by measuring the Stokes parameters $S_3(r,\phi)$ and $S_2(r,\phi)$. A similar measurement has been done in [21] by implementing an interferometer. The two intensity profiles, I_{45° and I_{135°, pertaining to S_2 can be measured behind a polarizer at angular orientations of 45° and 135° [as depicted in Fig. 1(a)] and those pertaining to S_3 (I_R and I_L) by introducing a preceding quarter-waveplate [as depicted in Fig. 1(b)]. Thus four measurements are required, and to date have been performed manually on static fields.

These four manual measurements can be reduced to two digital measurements, by replacing the quarter-waveplate and polarizer in Fig. 1(b) with a PG which acts as a beam-splitter for

#211246 - $15.00 USD Received 1 May 2014; revised 23 May 2014; accepted 23 May 2014; published 30 May 2014

right- and left-circular polarization, hence extracting I_R and I_L in a single measurement as shown in Fig. 1(d). Furthermore to measure the remaining two intensity profiles, I_{45° and I_{135°, a quarter-waveplate with its fast-axis set at 45° needs to be introduced before the PG to project I_{45° and I_{135° into the two detectable ports: I_R and I_L, respectively. Since a quarter-wave plate induces a quarter-wavelength phase shift on an incident beam thus converting linearly polarized light to circular and visa versa, this can be achieved by encoding the SLM with an additional $\pi/2$ phase term, as illustrated in Fig. 1(c). Previously, adjustments of the polarizer and quarter-waveplate would need to be made while acquiring measurements [Figs 1(a) and 1(b)]. However in our approach the necessary optics (PG and SLM) remain static and only a phase change is programmed on the SLM to mimic the required effect of a quarter-waveplate [Figs 1(c) and 1(d)].

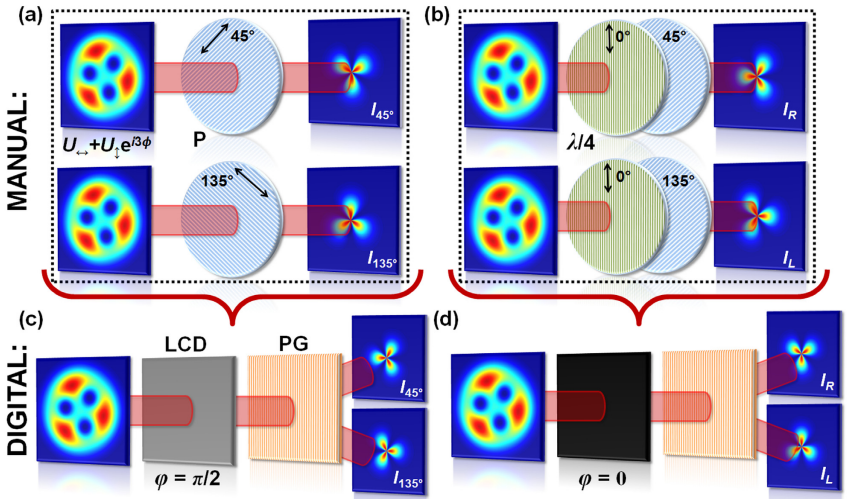

Fig. 1. A comparison between (a) and (b) the standard, manual Stokes polarimetry and (c) and (d) our corresponding digital method for extracting S_2 and S_3, respectively. The example illustrated here is an incoherent superposition of two Gaussian fields of orthogonal polarization where the vertical component has an additional azimuthal phase of $\exp(i3\phi)$. P: polarizer; $\lambda/4$: quater-waveplate; LCD: liquid crystal display of the SLM; and PG: polarization grating. Accompanying polarizer, quater-waveplate and LCD settings are given.

Apart from implementing this technique to extract the wavefront of unknown optical fields at a single plane, its use can be extended to investigate the field's wavefront at multiple planes along the beam's propagation. Traditionally this would be achieved by moving the wavefront sensing device transversely along the beam's propagation axis [illustrated in Fig. 2(a)]. Not only does the alignment become problematic (e.g., in the case of monitoring the trajectories of phase singularities), but it is also a time consuming procedure if many propagation steps are required. In a more advantageous approach we digitally simulate free-space propagation on the SLM [Fig. 2(b)]. This digital propagation technique [33] manipulates the spatial frequency spectrum of a beam of interest by first Fourier transforming the beam at the plane of the LCD with a lens and second by simultaneously displaying the phase term $\exp(ik_z z)$ on the SLM while implementing the inverse Fourier transform with a lens to the plane of the detector,

$$\mathscr{F}^{-1}(\mathscr{F}[U(r)]\exp(ik_z z)). \tag{7}$$

Merging these two digital methods (wavefront-sensing and propagation) together provides a

#211246 - $15.00 USD Received 1 May 2014; revised 23 May 2014; accepted 23 May 2014; published 30 May 2014

tool that does not require any information of the optical field under investigation as well as no moving optical components.

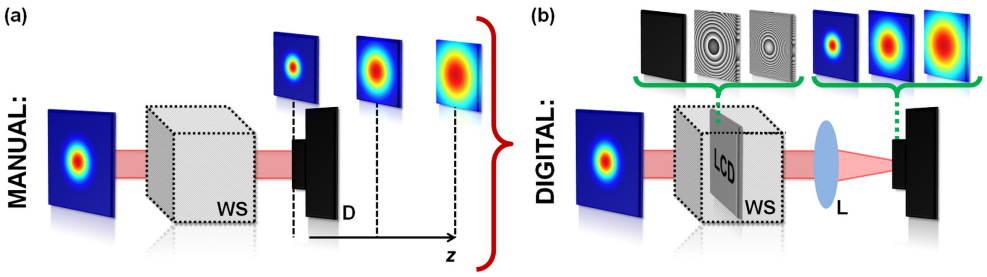

Fig. 2. A comparison between (a) the standard, manual movement of a detector along a beam's propagation and (b) the digital propagation method. The example illustrated here is a Gaussian beam. WS: wavefront-sensing technique consisting of a LCD and PG; D: detector; and L: lens. Accompanying intensity profiles and phase patterns encoded on the LCD for particular propagation distances (z) are given as inserts.

3. Experimental Methodology

To measure the wavefront of structured light beams we used an experimental setup as outlined in Fig. 3(a). A helium-neon laser (power $\sim$ 10 mW, $\lambda \sim 633$ nm) was expanded and collimated [$f(\mathrm{L}_1) = 20$ mm and $f(\mathrm{L}_2) = 100$ mm] to illuminate the LCD of a reflective SLM (Pluto Holoeye, 1920×1080 pixels, 8 μm pixel pitch, calibrated for $\lambda \sim 633$ nm) preceeded by a polarizer (P) to set the amplitudes of the two orthogonal states depicted in Eq. (1). The LCD was encoded with phase-only azimuthal [Fig. 3(b)], conical, cubic or random gray-level holograms to generate various structured light fields e.g. vortex, Airy, Bessel or speckle fields, respectively. The fields generated at the plane of the LCD were either Fourier-transformed (lens L_3) or relay-imaged (lenses L_4 and L_5) onto a CCD detector (PointGrey fire-wire CCD, 1600×1200 pixels), preceded by a PG, where the Stokes measurements, S_2 and S_3, were recorded. The PG which was placed $\sim$ 5 mm before the CCD detector, was manufactured by implementing a polarization holography setup where the sample was exposed with the interference of two plane waves each of opposite circular polarization. Since most phase-only holograms produce their corresponding fields in only the near-field (NF) or only the far-field (FF) and not both simultaneously, the two imaging systems (Fourier and relay) allowed the user to easily switch between the two and measure the wavefront of a variety of structured light beams. The Fourier-transforming imaging system also allowed the user to digitally simulate free-space propagation on the LCD (as defined in Eq. (7)), providing a means to extract the wavefront at multiple planes along the beam's propagation in real-time.

Since the LCD can be dynamically addressed, we first displayed the hologram required to create our field of interest [e.g. Fig. 3(b)] followed by the same hologram encoded with an additional $\pi/2$ phase term [e.g. Fig. 3(c)]. For each of the two holograms, the corresponding intensity profiles (I_{45°, I_{135° and I_R, I_L) were recorded to determine the two Stokes parameters, S_2 and S_3, respectively necessary for reconstructing the wavefront as defined in Eq. (6) and visualized theoretically in Fig. 3(d) and experimentally in Fig. 4. Similarly, this measurement was computed multiple times to extract the wavefront as the field was propagated by sequentially encoding the the phase term, $\exp(ik_z z)$, for various values of z while the necessary Stokes measurements were recorded.

The intensity profile of the field under investigation (i.e. the beam whose wavefront was being extracted) was viewed by encoding a blazed grating over the hologram [e.g. Fig. 3(e)]

#211246 - $15.00 USD Received 1 May 2014; revised 23 May 2014; accepted 23 May 2014; published 30 May 2014

with the PG removed from the setup. The desired, first diffraction order (with the reference, zero diffraction order removed) was then viewed on the CCD detector [e.g. Fig. 3(f)]. The propagation of the intensity profile was also monitored by sequentially encoding the phase term, $\exp(ik_z z)$, for various values of z together with the blazed grating.

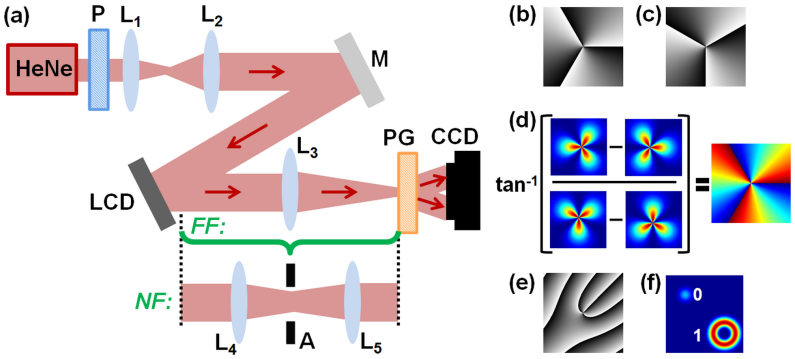

Fig. 3. (a) Schematic of the experimental wavefront sensing setup. HeNe: helium-neon laser; P: polarizer; $L_{1\to5}$: lenses; M: mirror; LCD: liquid crystal display of the SLM; A: aperture; PG: polarization grating; CCD: CCD detector. Example holograms for the azimuthal phase profile: (b) $\exp(i3\phi)$ and (c) $\exp(i3\phi+\pi/2)$ for the Stokes measurements, S_3 and S_2, respectively for extracting (d) the wavefront. (e) Example hologram (with a blazed grating) for extracting (f) the intensity profile.

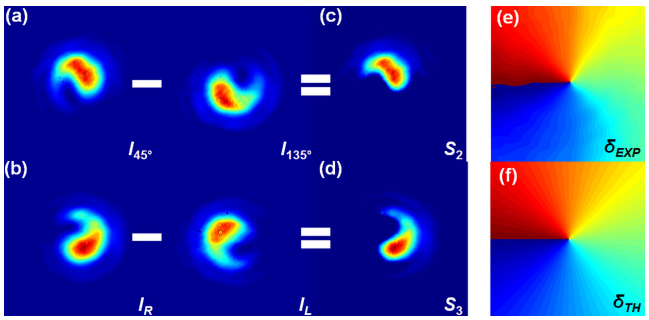

Fig. 4. Experimentally measured intensity profiles (a) I_{45°, I_{135° and (b) I_R, I_L (for a vortex beam of $\ell=+1$) used to calculate the Stokes parameters (c) S_2 and (d) S_3, respectively needed for the extraction of the (e) [(f)] measured (theoretical) wavefront.

4. Results and Discussion

The wavefronts of near-field, higher-order optical vortices [Fig. 5(a)] and Bessel beams [Fig. 5(d)] were measured via the digital Stokes polarimetry and are depicted in Fig. 5. It is evident that there is extremely good agreement between the experimentally extracted wavefronts, Fig. 5(b) [(e)], and the theoretically programmed phase profiles, Fig. 5(c) [(f)], for the vortex (Bessel) beams of azimuthal indices $\ell=-3$ to $+3$. Apart from identifying unit and higher-order phase singularities, this technique can also distinguish the handedness of the azimuthal phase profile [illustrated by the white arrows in Fig. 5(b)]. Closer inspection of the measured, higher-order ($|\ell|>1$) phase singularities reveals a separation into unit-charged singularities, denoted by the inserts in Figs 5(b) and 5(e). Even though the wavefront of the zero-order vortex

#211246 - $15.00 USD Received 1 May 2014; revised 23 May 2014; accepted 23 May 2014; published 30 May 2014

displays no curvature [less than a 1% variation and evident from the uniform, red wavefront in Fig. 5(b)], the splitting of the higher-order vortices is attributed to their fundamental instability.

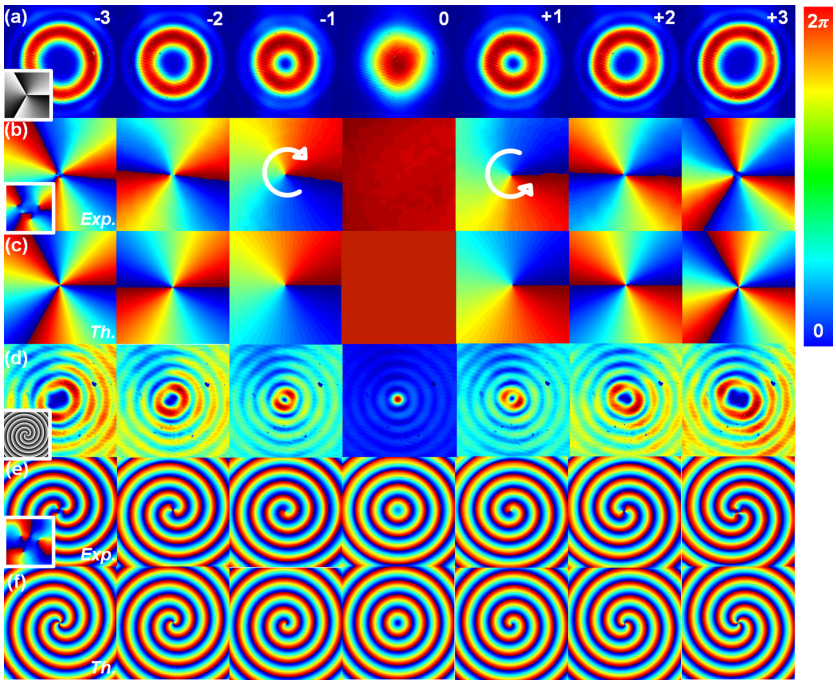

Fig. 5. Experimentally measured intensity profiles of (a) vortex beams and (d) Bessel beams. Some of the gray-level holograms used are given as inserts. Corresponding (b) [(e)] experimentally measured and (c) [(f)] theoretically calculated wavefronts for near-field vortex (Bessel) beams. The correlation between the measured and theoretical wavefronts varies from a minimum of 0.914 to a maximum of 0.988. Corresponding azimuthal indices are given in the top right corner. The white arrows highlight the handedness of the azimuthal phase. Inserts depict a magnified view of the singularities.

Similarly, the wavefront was extracted for an Airy beam [Fig. 6(a)] and a random speckle field [Fig. 6(b)] depicted in Figs 6(c) and 6(d), respectively with a high degree of fidelity with the theoretically encoded phase profile. Since the phase values of 0 (blue) and 2π (red) are indistinguishable, the line dislocation in the theoretical Airy wavefront can be neglected as seen in the measured wavefront [Fig. 6(c)].

The evolution of the wavefront for a Gaussian and vortex beam ($\ell = +2$) as they propagate was investigated and selected frames are shown in Figs 7(a) and 7(b), respectively. Unlike the previous results, these measurements were made in the far-field of the LCD plane [as illustrated in Fig. 3(a)] for the execution of the virtual propagation described in Eq. (7). One draw-back to performing Stokes polarimetry on the far-field mode is that the mode size is drastically smaller [by a factor of $f(\mathrm{L}_3)$] than that in the near-field, decreasing the resolution of the measured wavefronts. As the field propagates its wavefront becomes curved [evident in the frames of Fig. 7(a)] in agreement with the encoded phase profile [$\exp(ik_z z)$] which causes the two singularities in the vortex beam to move further away from one another, consequently appearing as if they are spirally around the beam axis [Fig. 7(b)].

#211246 - $15.00 USD Received 1 May 2014; revised 23 May 2014; accepted 23 May 2014; published 30 May 2014

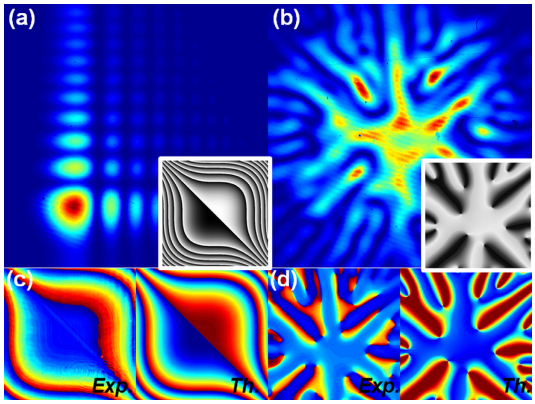

Fig. 6. Experimentally measured intensity profiles of an (a) Airy beam and (b) speckle field. The gray-level holograms used are given as inserts. Corresponding experimentally measured (Exp.) and theoretically calculated (Th.) wavefronts for a near-field (c) Airy beam and (d) speckle field.

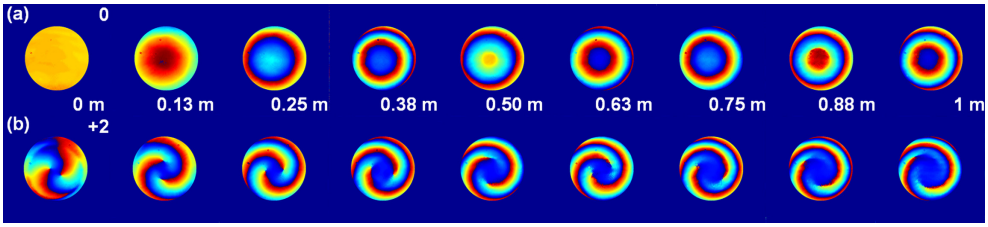

Fig. 7. Experimentally measured wavefronts for a (a) Gaussian and (b) vortex beam ($\ell = +2$) at different propagation planes. Corresponding propagation distances are given in the bottom right corner. The full data (video) can be viewed in (a) (Media 1) and (b) (Media 2).

5. Current Capabilities and Future Improvements

Although our wavefront sensor implements custom optics such as the PG, it offers many advantages. Firstly, our approach can be used to measure the wavefront of propagating light fields, over extended distances, with a single static device [evident in the video clips: (Media 1) and (Media 2)]. Since the necessary holograms can be addressed to the SLM at very high refresh rates [34], we are capable of extracting real-time measurements within a time-frame of a few milliseconds. To further increase this time frame, multiple holograms could be addressed via multiplexing [35] to allow the extraction of multiple measurement parameters in a single acquisition. We also propose that our approach could be combined with a current wavefront extraction technique (also based on SLM technology) known as modal decomposition [16, 17, 36]. This will allow one to decompose arbitary laser modes to yield an all-digital wavefront extraction technique for unknown beams.

Another appeal of our wavefront sensing technique is that the CCD detector defines the resolution of the reconstructed wavefront. Even though the PG (positioned before the CCD) splits the beam, projecting each diffraction order to a detector area of half the original spatial resolution, our approach offers a spatial resolution of 10^6 sample points as opposed to devices based on lenslet arrays which currently only offer a resolution of 10^4 sample points. Furthermore, this technique does not necessitate that we restrict ourselves to a single detector thus offering an ad-

#211246 - $15.00 USD Received 1 May 2014; revised 23 May 2014; accepted 23 May 2014; published 30 May 2014

ditional improvement in spatial resolution. With this high spatial resolution we can identify the position and topology of closely spaced phase singularities in random speckle fields [evident in Fig. 6(d)]. This approach will allow one to experimentally verify current numerical studies of phase singularities propagating through atmospheric turbulence [37].

6. Conclusion

In conclusion, we have presented a new approach to conventional Stokes polarimetry that results in an all-digital, adjustment-free measurement of the wavefront of propagating structured light beams. As the digital holograms are dynamical addressed, the technique can be executed at refresh rates of 250 Hz to yield real-time wavefront measurements at various planes along the beam's propagation. We have successfully demonstrated this tool on beams that are usually difficult to analyse with traditional wavefront sensing techniques, namely, Airy, Bessel, vortex and speckle fields, while observing dynamic changes in their wavefronts during propagation. Since we are able to reconstruct wavefronts with high spatial resolution and fidelity, we suggest our diagnostic could be a versatile tool in numerous areas such as studies into the creation and annihilation of phase singularities, microscopy and free space communication.

Acknowledgments

We gratefully acknowledge the manufacturing of the PG from the Opto-Electronics and Lightwave Engineering Group at North Carolina State University. A. D. acknowledges support from CSIR YREF Grant Ref. YREF 2014 019. G. M. and R. R. A. acknowledge support from ARO Grant. No. 47221-00-01, ARO Grant. No. 52759-PH-H, NSF GRFP Grant. No. 40017-00-04, and Corning, Inc. A. F. acknowledges support from NRF Grant. No. 78977.

#211246 - $15.00 USD Received 1 May 2014; revised 23 May 2014; accepted 23 May 2014; published 30 May 2014